International Journal of Engineering Research and Science & Technology

www.ijerst.org

ISSN : 2319-5991

Vol. 22 No. 1(s) (2026)



ijerst.editor@gmail.com

editor@ijerst.com

www.ijerst.com
© 2026 IJERST. All Rights Reserved
Peer Reviewed, Referred & Indexed Journal

Research Paper

Impact of annealing temperature on Ta_2O_5 nanostructure and photocatalytic degradation of Basic Fuchsin dye

Akshay Mahapure[a], Akash Nagare[a], Amol Dhadage[a], Durga Bharat[a], Deepak Shinde[a], Madhukar Navgire[b], Anil Athare[a], Ramesh Naval[b*]

[a]New Arts, Commerce and Science College, Ahmednagar, Maharashtra, PIN-414001,

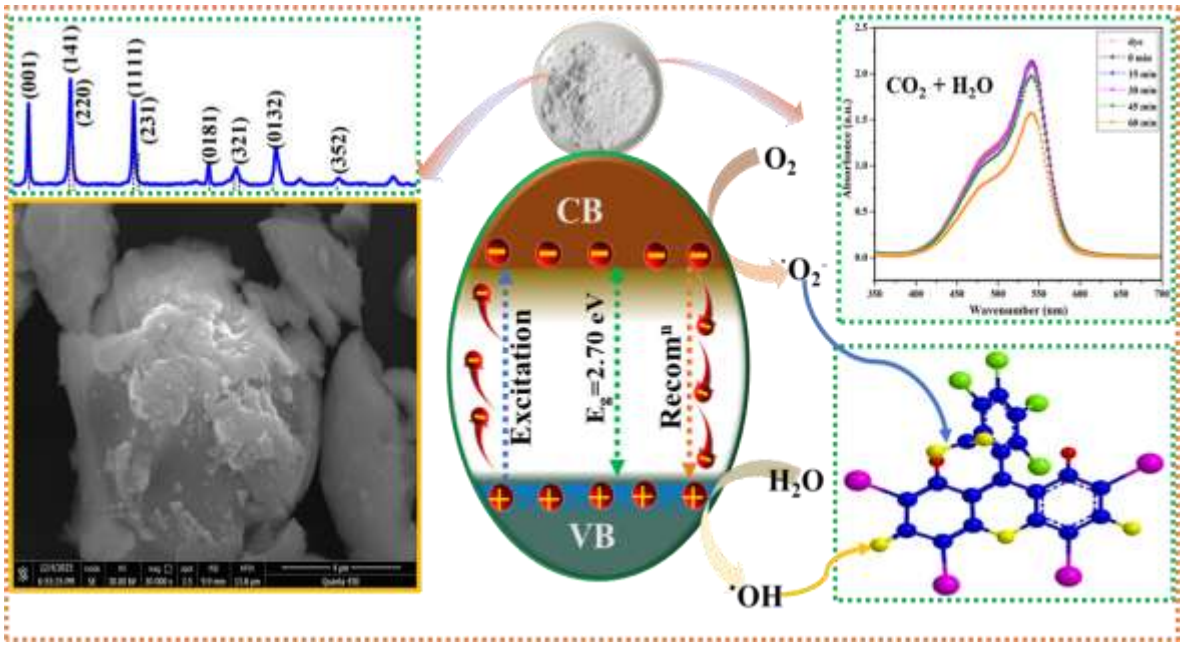
[b]Jijamata College of Science and Arts, Bhende, Maharashtra, PIN-414605.

*Corresponding author: Ramesh Naval (rameshnaval@gmail.com)

Abstract

Ta_2O_5 nanoparticles are synthesized by using sol gel technique. Further the synthesized material calcined at various temperature like 500 °C, 600 °C and 700 °C and indicated by T5, T6, and T7 respectively. First phase changes from hexagonal to orthorhombic phase identified by using X- ray diffraction spectra. As a result, observed by optical bandgap very close to theoretical value. FTIR spectroscopy examines the vibrational characteristics of the material. FE-SEM displayed hexagonal like shape. XPS spectra results shows confirm the elemental composition and identified oxygen vacancies. Further towards the application parts of photocatalytic activity. Among the 600 °C nanoparticle shows 41% degradation under the sunlight over 60 minutes results for basic fuchsin dye.

Graphical abstract



Highlights

- T5, T6 and T7 were synthesized by sol-gel technique.
- T5 and T6 shows hexagonal Ta_2O_5 phase while T7 shows orthorhombic phase.
- The 41% of BF dye degrade in 60 minutes for T6 material.

Keywords Temperature variation, Ta_2O_5, Sol-gel, Photocatalytic degradation.

1 Introduction

In recent years environmental pollution has emerged as a critical problem around the world. It attracts attention of scientist due to the pollution is seen to be major problem. This problem mainly comes from the use of different synthetic dyes for the particular textiles [1][2]. During the dyeing process, due to chemical interaction, an unfixed dye release into wastewater [3]. Triphenylmethane dyes which includes crystal violet, malachite green and basic fuchsin are highly used due to low cost [4]. Also, they used for the coloration of various material like nylon, cotton, wool, and silk [5]. Various techniques have been established to reduced that wastewater pollution contains physicochemical processes such as coagulation and photocatalytic degradation [6][7].

The basic fuchsin dye exhibits low biodegradability, leading to its accumulation in water bodies and increasing risk of chronic exposure [8]. That dye has there possible carcinogenic, genotoxic and neurotoxic affects, also it harms kidney and liver tissues [9][10]. Moreover, basic fusion dye affects the aquatic organism and biodiversity. This situation underscores the urgent need to developed effective remediation.

For the purpose to deals with the risks associated with basic fuchsin dye, a variety of physicochemical and biological treatment approaches have been investigated. That includes membrane filtration, bioremediation and adsorption. Out of all that methods adsorption is a effective technique in removing dyes even at very low concentration.

Tantalum oxide shows properties like electronics, optics and photocatalysis [11]. Ta_2O_5 shows an eco-friendly nature due to its chemical stability, corrosion resistance, and non-toxicity [12][13]. Ta_2O_5 material has a wide bandgap; it shows photocatalytic efficacy in the UV region as compared to visible light to enhance that photocatalytic efficacy with calcination at various temperatures studied in the present work.

Synthesis of Ta2O5 using simple sol-gel method at different temperature ranges from 500°C, 600°C, and 700°C and characterized using different analytical methods, i.e., XRD, FE-SEM, FTIR, UV-DRS and XPS. These studies particularly connect optical and structural changes to photocatalytic activity. This study reports an important void in existing works and introduces an innovative approach to activate wide-bandgap oxides for operations under

visible light calcined at various temperature 500°C, 600°C, and 700°C for 3 hours and labelled it as T5, T6 and T7 respectively.

2 Experimental methods

2.1 Experimental section

Tantalum chloride ($TaCl_5$) was purchased from LOBA Chemicals Pvt. Ltd. The precipitating agent was ammonia solution (NH_4OH), and the surfactant was cetyltrimethylammonium bromide, ($C_{19}H_{42}N.Br$), both of which were acquired from SD Fine Chemicals. Basic fuchsin dye ($C_{20}H_{19}N_3 \cdot HCl$), hydrogen peroxide ($H_2O_2$), and all chemicals used are of A. R. grade. Double-distilled water (DDW) was used for all experimental methods.

2.2 Synthesis of Ta_2O_5 NPs:

By using a simple sol-gel technique pristine Ta_2O_5 material were synthesized. Initially, tantalum pentachloride ($TaCl_5$) precursor was slowly added to double distilled water under continuous stirring in a beaker. 0.2 g of cetyl trimethyl ammonium bromide (CTAB) was introduced to regulate surface development. The solution was maintained at a temperature of 40 °C and stirred at 250 rpm for 3 hours resulting in the development of a stable gel. The resulting gel was aged then next step is drying in an oven at 80°C for 12 hours and calcined Ta_2O_5 NPs 500°C, 600°C, and 700°C for 3 hours and labelled it as T5, T6 and T7 respectively.

2.3 Photocatalytic activity

Under direct sunlight the photocatalytic dye degradation activity was performed for the BF dye. During this activity 50 ml of 10 ppm BF dye solution was prepared to performed an experiment. Initially the dye solution was put in the dark for 30 minutes to carryout adsorption desorption phenomenon. Then 10mg photocatalyst and 2ml of 10ppm H2O2 was added to the dye solution and put that solution directly under the sunlight for 150 minutes. At equal interval 15 minutes records the absorbance by using UV- spectrophotometer and plot the graph using origin.

2.4 Characterization

A different analytical technique was used for characterization. The bandgap energy was calculated using a Lab India UV-vis spectrophotometer (UV 3092). The Thermofisher NEXA surface analyser with an Al Kα X-ray source, X-ray Photoelectron Spectrum for measuring the binding energy of Ta2O5 material. The PerkinElmer (Spectrum 2) spectrometer analysed the vibrational properties of material. X-ray diffractometer (Rigaku Ultima IV 600) utilized Cu Kα (λ=0.15418 nm) radiation, operating at a scan rate of 2

degrees per minute, to identify phase and structural properties. Surface morphology was analysed using FE-SEM (Nova Nano Sem 450). The breakdown of the dye BF using light was measured with a UV-VIS spectrophotometer (Double Beam UV-VIS Spectrophotometer AU 2701).

3 Result and Discussion

3.1 X-ray diffraction (XRD) analysis

The XRD patterns of T5, T6, and T7 are displays in figure 1. In figure 1(a) and 1(b) characteristic peaks observed at 2θ values of 22.96°, 28.44° and 36.86° are indexed to the (003), (200) and (203) planes, respectively, which are in good agreement with the standard JCPDS card No. 18-1304, corresponding to the hexagonal Ta_2O_5 phase with lattice parameters a = 7.24 Å, b = 7.24 Å, and c = 11.61 Å.

In figure 1(c) characteristic peaks observed at 2θ values of 22.85°, 28.45° and 29.17°, are indexed to the (001), (141) and (1111) planes, respectively, which are in good agreement with the standard JCPDS card No. 25-0922, corresponding to the orthorhombic Ta_2O_5 phase with lattice parameters a = 6.198 Å, b = 40.29 Å, and c = 3.888 Å.

$$D = \frac{K\lambda}{\beta COS\theta} \qquad (1)$$

Where k represents shape factor, **λ** is the incident wavelength, θ represents Bragg angle, and β denoted FWHM. Enhancement in peak intensity and sharpening is observed, by increasing calcination temperature from T5 to T7, indicating improved Crystallite Size. Impurity phases are not noticed, confirming the phase purity and structural stability of Ta_2O_5 across the studied calcination temperatures.

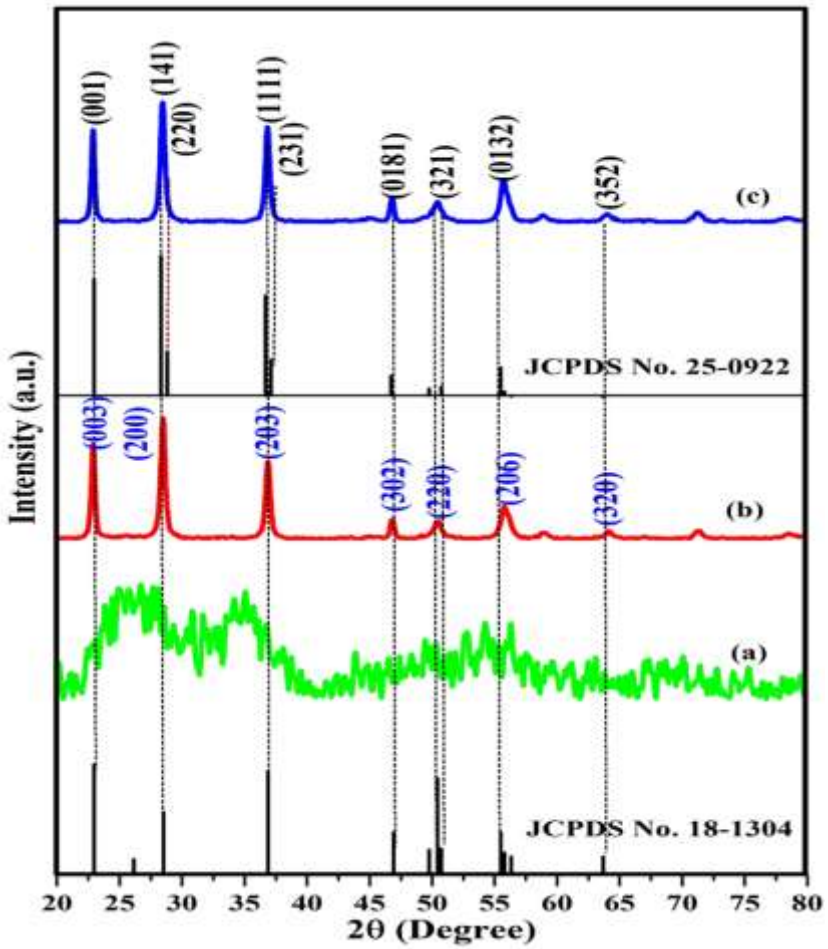


Figure 1 XRD pattern of synthesized (a) T5, (b) T6, and (c) T7 material

Table 1 Crystallite size (D) of synthesized materials

Sr. No	Materials	Crystallite Size D (nm)
1.	T5	44.47
2.	T6	56.52
3.	T7	62.62

3.2 Fourier transform infrared (FTIR) analysis

Figure 2 displayed spectra of FTIR the T5, T6 and T7 at 500 °C, 600 °C and 700 °C. The 405 cm^{-1} and 510 cm^{-1} absorption bands associated to bending vibration and stretching vibration Ta-O. The band at 600 cm^{-1} is associated to the Ta-O-Ta bridging vibration and Ta=O stretching modes are observed at 500 °C and 600 °C. Furthermore, 780 to 820 cm^{-1} at 700 °C were contributed to the vibration of Ta-O-Ta bonds, representing the transformation from the hexagonal phase to the orthorhombic Ta_2O_5 phase and band appearing near 890 to 910 cm^{-1} is associated to the adsorption of O2- species and Ta=O stretching vibrations on the Ta_2O_5 surface. Generation of oxygen vacancies during the variation of temperature it

enhanced adsorption of oxygen by changing the Ta-O coordination environment. High purity of T5, T6 and T7 was observed in FTIR due to the no additional peak observed.

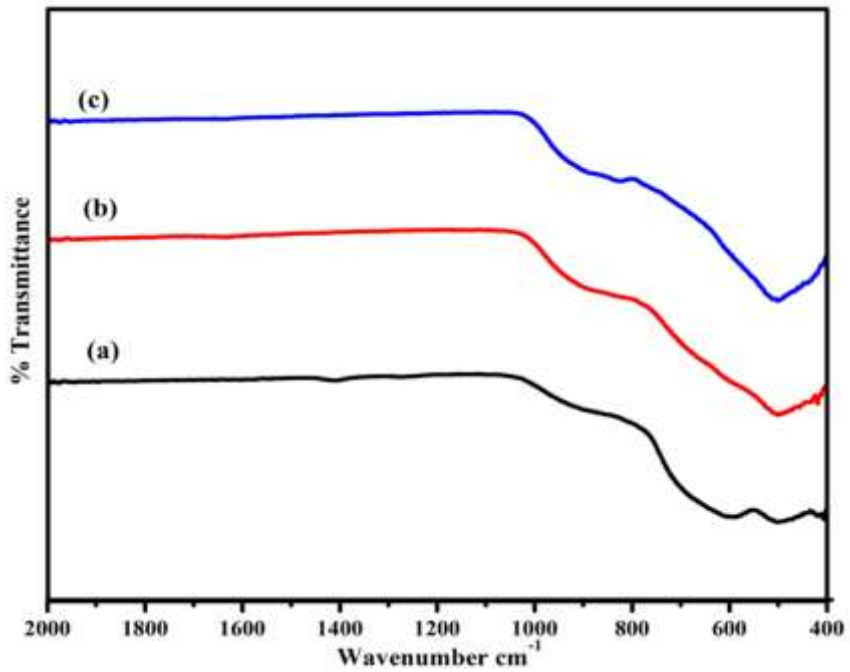


Figure 2 FTIR spectra of (a) T5, (b) T6, and (c) T7 material

3.3 Field emission scanning electron microscopy (FE-SEM) analysis

FE-SEM technique was employed to analyse surface morphology of T6 material. Figure 3 displayed formation of nano disk like structures. Using EDS and elemental mapping reveals a uniform distribution and the presence of elements Ta and O, with no other impurities observed.

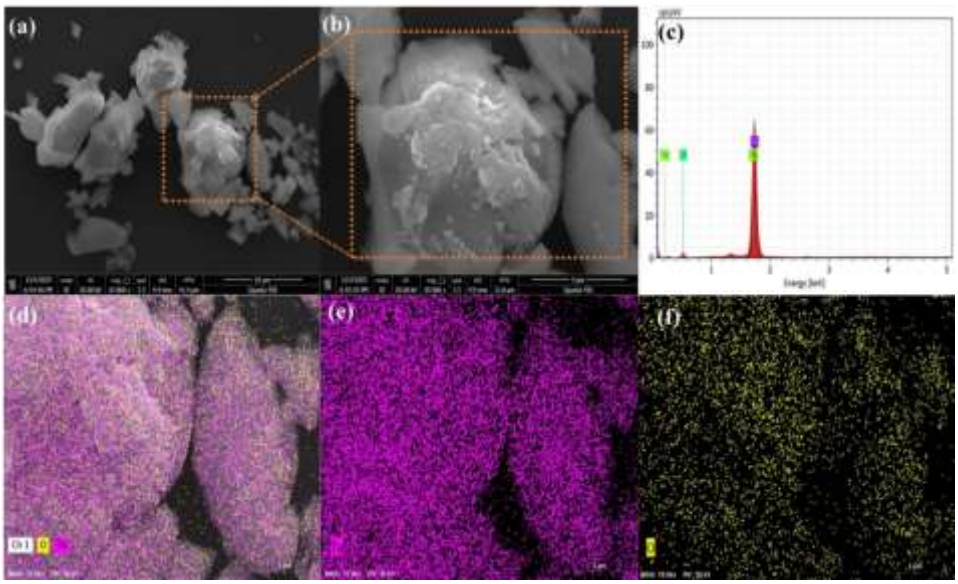


Figure 3 (a-b) SEM micrographs of T6 material, (c) EDS spectrum of T6 material, (d-f) color mapping of T6 material

3.4 X-ray photoelectron spectroscopy (XPS) analysis

The oxidation state and surface chemical composition of T6 was examined using XPS displayed in figure 4(a) Purity of synthesized material indicating Ta and O demonstrated by survey spectrum. The Ta^{5+} species illustrated in figure 4(d) are corresponds to a doublet of 26.31 eV at (Ta $4f_{7/2}$) and 28.15 eV at (Ta $4f_{5/2}$) [14]. Figure 4(b) exhibits C 1s spectrum of synthesized material, peaks at 288.5 eV, 286.7 eV, and 284.7 eV binding energies corresponds to (C=O), (C-O), and (C-C). Lattice oxygen is contributing for the peak having binding energy 530.5 eV displayed in figure 4(c). As surface reactivity of synthesized material increases with increasing number of oxygen vacancies, leading to more activity in photocatalytic dye degradation.

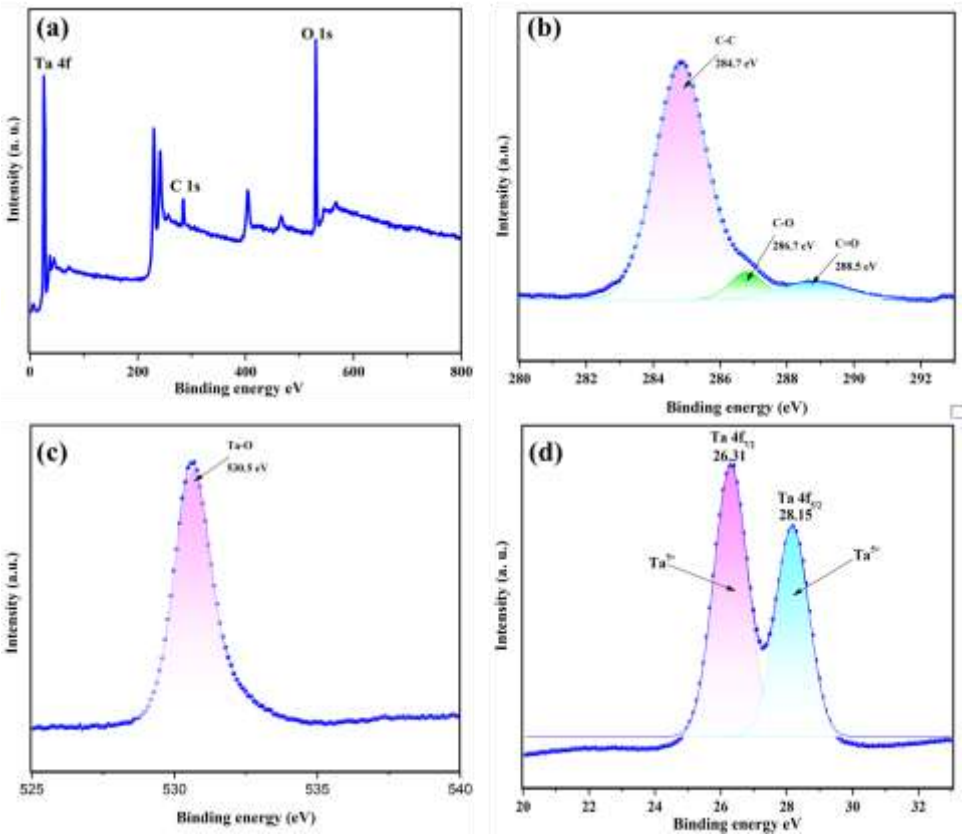


Figure 4 (a) XPS survey spectra of T6 material, (b) C 1s, (c) O 1s, and (d) Ta 4f

3.5 UV-visible diffused reflectance spectroscopy (UV-DRS) analysis

The optical bandgap calculated by using UV-DRS as shown in figure 5. T6 has optical bandgap 2.70 eV which improved absorption of visible light as compared to T5 and T7 [15]. This reduction in bandgap results from formation of defect states induced by oxygen vacancies during the calcination which is responsible for photon absorption. Similarly, T5 (3.03 eV) has limited defect formation, whereas T7 (3.18 eV) corresponds to high crystallinity and reduction of defects. Temperature variation affects the bandgap energy confirm by using Tauc plots.

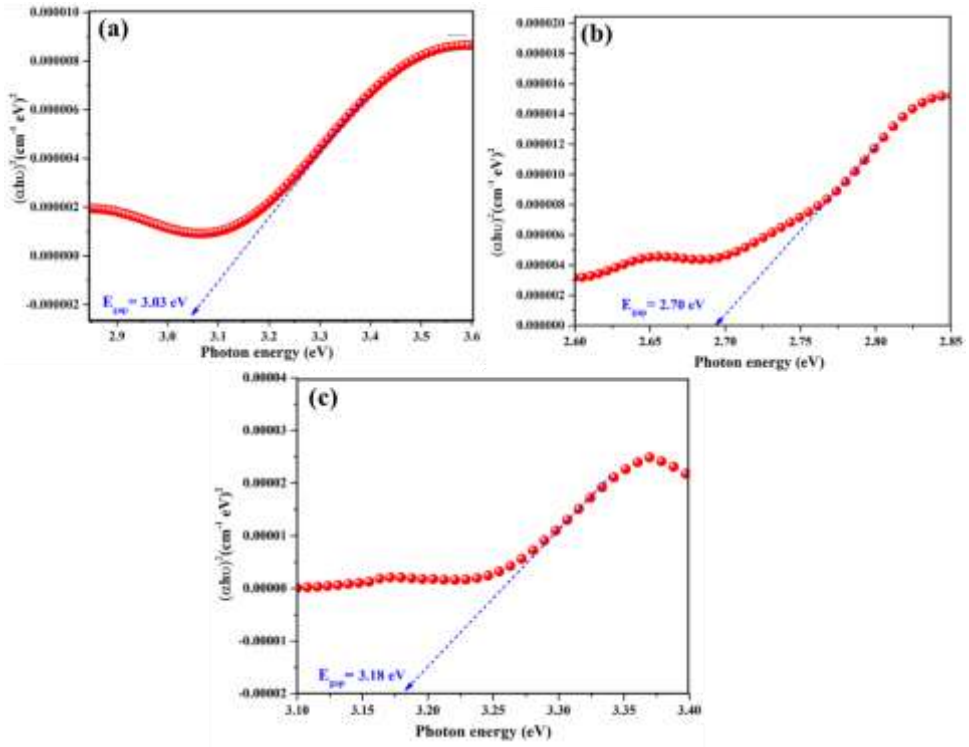


Figure 5 UV-DRS spectra of (a) T5, (b) T6, and (c) T7 material

Table 2 Bandgap energy, valence band potential and conduction band potential for T5, T6, and T7 material

Sr. No.	Materials	Bandgap (eV)	E_{VB}	E_{CB}
1	T5	3.03	3.57	0.54
2	T6	2.70	3.41	0.70
3	T7	3.30	3.65	0.47

4 Photocatalytic activities of synthesized material

Using BF dye photocatalytic degradation performance was assessed under the sunlight. By using equation (4) degradation efficiency was determined.

$$E = \frac{C_0 - C_t}{C_0} \times 100 \quad (2)$$

$$C_t - C_0 = e^{-kt} \quad (3)$$

$$\ln\left(\frac{C_0}{C_t}\right) = kt \quad (4)$$

Where, C_t and C_0 indicates the dye concentration at the moment of irradiation time and initial dye concentration before the photocatalytic reaction, respectively. The photocatalytic degradation of BF dye of T5, T6, and T7 materials was thoroughly investigated under sunlight, as displayed in figure 6. The aqueous BF dye solution showed less degradation even after 30 minutes under the sunlight in absence of the photocatalyst.

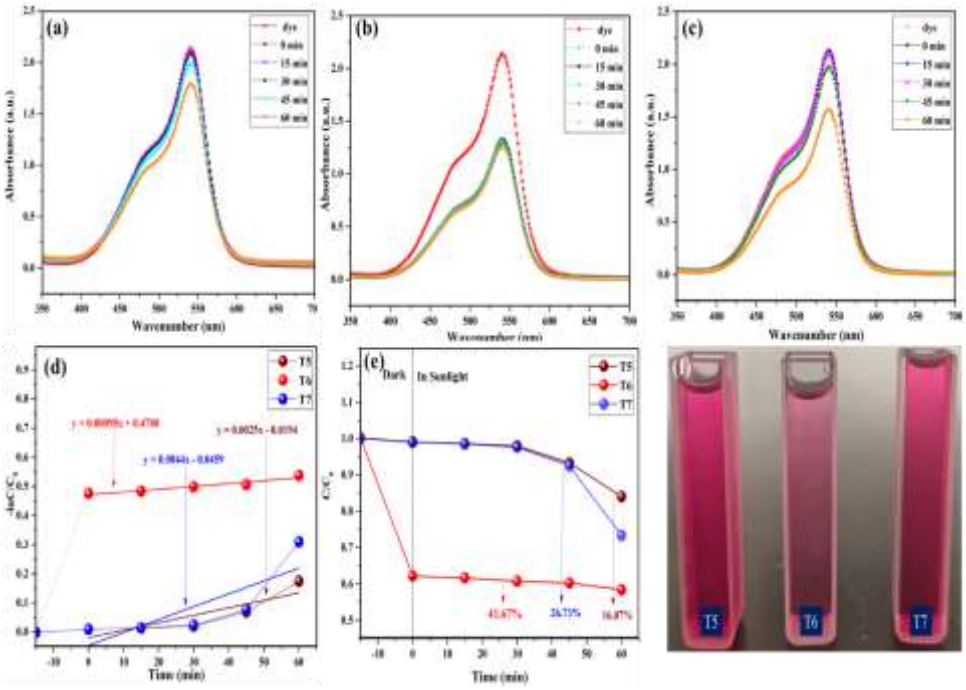


Figure 6 Absorption spectra of BF dye in (a) T5, (b) T6, and (c) T7 material, (d-e) Rate kinetics for T5, T6, and T7 material (f) Colour change for T5, T6, and T7 material

In this study the photocatalytic degradation of 16%, 41%, and 26% in 60 minutes for T5, T6, and T7 nanomaterials was observed under the sunlight displayed in figure 6(e). These adsorption values can be related with the optical bandgap of photocatalyst. The T5 material have bandgap 3.03eV having E_{VB} and E_{CB}, 3.57 and 0.54. whereas the T6 material has bandgap 2.70 eV with E_{VB} and E_{CB}, value is 3.41 and 0.70. Moreover, T7 material has bandgap 3.30 eV with E_{VB} and E_{CB}, value is 3.65 and 0.47. As compared to T5, T6 and T7, T6 has less optical bandgap value which increases photocatalytic degradation. Also, by comparing E_{VB} and $E_{CB,}$ values for T6 has less E_{VB} and higher E_{CB} value which promoted to the generation of e^-- h^+ pairs.

Table 3 Rate kinetics for T5, T6, and T6 materials

Sr. No.	Materials	Rate constant	Equation
1	T5	0.0057	y= 0.0025x - 0.0194
2	T6	0.0022	y= 0.00098x + 0.0415
3	T7	0.0100	y= 0.0044x - 0.0459

5 Photocatalytic mechanisms

Figure 7 displays the mechanism of photocatalytic dye degradation of T6 material under direct exposure of sunlight. When the optical bandgap of synthesized T6 material is less than the proposed light that responsible for the creation of photogenerated e^-/h^+ pairs. T6 nanomaterial has low bandgap (2.70) as compared to T5 and T7. By using Butler's formula

conduction band (CB) position and valence band (VB) position are calculated as shown in Table 2.

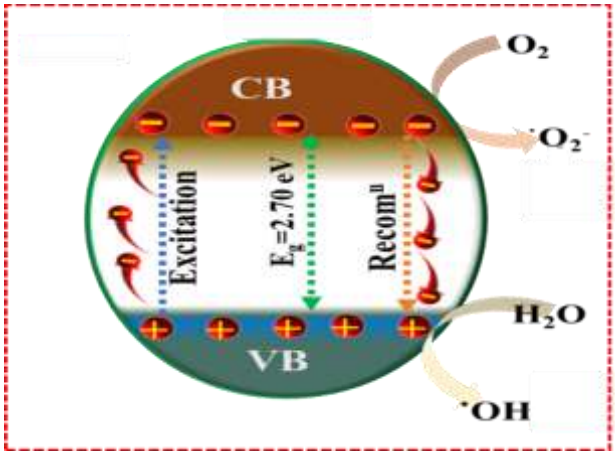


Figure 7 Mechanism of photocatalytic activity .

Conclusions

Due to the calcination of Ta_2O_5 at 500 °C, 600 °C and 700 °C it affects the functional and structural properties. At 500 °C, Ta_2O_5 (T5) shows amorphous nature having low crystallite size with high defect density. As the calcination temperature increases to 600 °C, Ta_2O_5 (T6) results the hexagonal Ta_2O_5 which enhanced structural arrangement and relation between crystallite size and defects, leading to better functional performance. Further calcination at 700 °C orthorhombic Ta_2O_5 (T7) results high crystallite size with low defect density, which enhanced structural arrangement leads to decrease in photocatalytic activity attributed to decreased surface area and defect-mediated charge trapping. These results described that T6 has application in environmental remediation.

References

1) A. Dhadage, A. Nagare, P. Ghare, A. Athare, P. Gogoi, and M. Navgire, "Ultrasonic wave-assisted synthesis of CeO2-MoO3 nanocomposite for photo-Fenton degradation of Rhodamine-B dye," Chemical Papers, vol. 78, no. 10, pp. 5833–5850, Jul. 2024, doi: 10.1007/s11696-024-03479-2.
2) A. H. Al-Marri et al., "Enhanced photocatalytic properties of the Nb2O5/rGO for the degradation of methylene blue," Ionics (Kiel)., vol. 29, no. 12, pp. 5505–5515, Dec. 2023, doi: 10.1007/s11581-023-05255-w.
3) M. A. Rauf and S. S. Ashraf, "Fundamental principles and application of heterogeneous photocatalytic degradation of dyes in solution," Aug. 15, 2009. doi: 10.1016/j.cej.2009.02.026.
4) Z. Boutamine et al., "The investigation of the basic fuchsin dye photocatalytic degradation in aqueous media using stabilised Span 80 and synthesized ultrasonically CuO Nanoparticles (NPs)," Reaction Kinetics, Mechanisms and Catalysis, vol. 138, no. 3, pp. 1813–1832, Jun. 2025, doi: 10.1007/s11144-025-02806-2.
5) T. S. Munonde, N. P. September, A. Mpupa, and P. N. Nomngongo, "Two agitation routes for the adsorption of Reactive Red 120 dye on NiFe LDH/AC nanosheets from wastewater and river water," Appl. Clay Sci., vol. 219, Mar. 2022, doi: 10.1016/j.clay.2022.106438.
6) I. Khemissi, R. Laajimi, K. Ben Mabrouk, A. Hajjaji, and M. Rahmani, "An in-depth study by machine learning models of the absorbance properties of stable Ta2O5 nanotubes decorated by

PbS nanoparticles for photocatalytic applications," Mater. Res. Bull., vol. 184, Apr. 2025, doi: 10.1016/j.materresbull.2024.113247.

7) S. Dutta and J. Bhattacharjee, "A comparative study between physicochemical and biological methods for effective removal of textile dye from wastewater," in Development in Wastewater Treatment Research and Processes: Innovative Microbe-Based Applications for Removal of Chemicals and Metals in Wastewater Treatment Plants, Elsevier, 2021, pp. 1–21. doi: 10.1016/B978-0-323-85657-7.00003-1.
8) H. Ahmed et al., "Efficient Removal of Basic Fuchsin from Synthetic Medical Wastewater and Competitive Adsorption in the Mixture," Adsorption Science and Technology, vol. 2023, 2023, doi: 10.1155/2023/4672622.
9) A. Taamallah, S. Merouani, and O. Hamdaoui, "Sonochemical degradation of basic fuchsin in water," Desalination Water Treat., vol. 57, no. 56, pp. 27314–27330, Dec. 2016, doi: 10.1080/19443994.2016.1168320.
10) E. A. Abdelrahman, "Efficient adsorption of basic fuchsin dye using thermally engineered novel smart nanocomposites," Sci. Rep., vol. 15, no. 1, Dec. 2025, doi: 10.1038/s41598-025-12348-1.
11) J. Zheng, Z. Li, M. Zhang, and T. Zhang, "Enhancing reflectivity of tantalum oxide coatings through plasma spraying and annealing techniques," Mater. Lett., vol. 378, Jan. 2025, doi: 10.1016/j.matlet.2024.137585.
12) E. Mendoza-Mendoza et al., "A novel two-step route for synthesizing pure Ta2O5 nanoparticles with enhanced photocatalytic activity," Ceram. Int., vol. 45, no. 5, pp. 6268–6274, Apr. 2019, doi: 10.1016/j.ceramint.2018.12.108.
13) D. V. Mashtalyar et al., "Effect of Ta2O5 nanoparticles on bioactivity, composition, structure, in vitro and in vivo behavior of PEO coatings on Mg-alloy," Journal of Magnesium and Alloys, vol. 12, no. 6, pp. 2360–2379, Jun. 2024, doi: 10.1016/j.jma.2024.06.014.
14) H. L. Huang, M. T. Tsai, Y. J. Lin, and Y. Y. Chang, "Antibacterial and biological characteristics of tantalum oxide coated titanium pretreated by plasma electrolytic oxidation," Thin Solid Films, vol. 688, Oct. 2019, doi: 10.1016/j.tsf.2019.04.043.
15) A. Gupta, L. K. Brar, S. Jaidka, K. M. Kamal, S. Gyergyek, and B. Likozar, "White LED - Driven hydrogen production: Tantalum oxide supported g-C3N4 sheets as a Pt-free catalyst," Int. J. Hydrogen Energy, vol. 130, pp. 423–433, May 2025, doi: 10.1016/j.ijhydene.2025.04.370.